Shell model study of backbending phenomena in Xe isotopes

K. Higashiyama,* N. Yoshinaga,† and K. Tanabe‡
Department of Physics, Saitama University, Saitama City 338-8570, Japan
(Received 30 December 2001; published 9 May 2002)

Xe isotopes near mass $A\sim130$ region, which exhibit features of O(6) symmetry at low energy and the backbending at high spins, are studied in the shell model framework. The monopole and quadrupole pairing plus quadrupole-quadrupole interaction is employed as an effective interaction. As for single-particle levels, the $1d_{3/2}$, $0h_{11/2}$, $2s_{1/2}$ orbitals are taken into account for neutrons and the $1d_{5/2}$, $0g_{7/2}$ orbitals for protons under the assumption of $N=Z=64$ subshell closure. The calculation reproduces the experimental energy levels of high-spin states as well as low-lying states well. This is the first successful microscopic description of the backbending in this mass region. The shell model states are examined in pair-truncated models. The analysis shows the alignment of two $0h_{11/2}$ neutrons at high spins.

DOI: 10.1103/PhysRevC.65.054317 PACS number(s): 21.10.Re, 21.60.Cs, 21.60.Ev, 27.60.+j

I. INTRODUCTION

There exist two prominent features in nuclei with mass $A\sim130$. First, the backbending phenomena are observed in many of the nuclei in this region. The basic mechanism of the phenomena has been regarded as a quasiparticle level crossing between an unoccupied high-j intruder orbital and the most high-lying occupied orbital, causing a sudden increase of moment of inertia along the yrast level sequence. Secondly, the energy scheme shows a feature of the γ instability in low-lying states, which is known as a manifestation of O(6) symmetry in the interacting boson model (IBM) [1]. This feature becomes manifest in the energy staggering of even-odd spin states in the quasi-γ band and also in some forbidden $E2$ interband transition rates. To describe consistently these aspects in terms of a completely microscopic framework is an important and intriguing issue in the transitional nuclei.

The IBM describes collective properties of low-lying nuclear states in terms of its angular momenta zero (s) and two (d) bosons. Low-lying states in the $A\sim130$ nuclei were extensively studied in terms of the IBM, and energy spectra and electromagnetic transitions were successfully described [2,3]. A similar study was carried out using the fermion dynamical symmetry model (FDSM) [4]. The low-lying states were also well reproduced in terms of the FDSM. However, the model has deficiencies that structure of pairs is fixed irrespective of dynamics and that the contribution of single-particle energies within the k-i basis is a constant.

Recently, the nucleon-pair shell model (NPSM) [5,6] was introduced to incorporate dynamics in determining the structure of pairs. The model essentially reduces to the SD-pair model [7–11] except some details in mathematical treatment, provided that the pairs in the NPSM are restricted to the angular momenta zero (S) and two (D) pairs. However, the NPSM with S and D pairs is not successful in describing high-spin states [12–14] because decoupling of the pairs with higher angular momenta is a predominant mechanism of the structure change in the high-spin states near the backbending region. Thus, previous studies were successful only in the low-lying states [2–4,11–15], but they are not enough for high-spin states without decoupled pairs.

Microscopic studies of the backbending phenomena have been carried out in terms of mean field frameworks. Various cranked Hartree-Fock-Bogoliubov calculations using the pairing plus quadrupole-quadrupole type interaction [16–19], the Gogny interaction [20,21], and the Skyrme interaction [22,23] have described the backbending phenomena successfully. However, very few studies were made from the shell model point of view. The reason is stated as follows. While most medium-heavy nuclei with a large number of nucleons show the backbending, applications of the shell model were restricted to light nuclei with a few valence nucleons since the dimension of the configuration space becomes prohibitively huge for heavier nuclei. Though the number of studies is limited, in lighter nuclei there exist a couple of studies of the backbending in the shell model framework. For example, the backbending calculations were carried out for ^{48}Cr and ^{50}Cr, and the even-spin yrast sequences were reproduced quite well [24,25]. The mechanism of the backbending for ^{48}Cr was investigated in terms of the projected shell model and the generator coordinate method [26].

The IBM was extended by including the fermionic intruder configurations [27,28]. Backbending calculations around the $A\sim130$ region were carried out on the basis of this extended IBM [27–30]. Although it was a very important attempt, the model cannot deal with the Pauli principle explicitly between the boson core and the fermionic intruder configurations. To take into account the Pauli effect explicitly, we introduce a model of the SD pairs with a neutron $(h_{11/2})^2$-pair as an improved model of the extended IBM by replacing the s and d bosons by the S- and D-collective fermionic pairs.

In this paper we describe in a comprehensive manner the nuclear states from low spins to high spins, where the former indicate the γ instability and the latter display the backbending phenomena, using both the full-fledged shell model and pair-truncated models. In the practice of calculations, we employ the monopole and quadrupole pairing plus quadrupole-

*Electronic address: higashi@phy.saitama-u.ac.jp
†Electronic address: yosinaga@phy.saitama-u.ac.jp
‡Electronic address: tanabe@phy.saitama-u.ac.jp

quadrupole interaction ($P+QQ$) as an effective interaction. The model space is restricted to $64 \leqslant N \leqslant 82$ ($50 \leqslant Z \leqslant 64$) for neutrons (protons) under the assumption of $N=Z=64$ subshell closure for the feasibility of our shell model calculation.

In Sec. II, shell model calculations for $^{130-136}_{54}$Xe isotopes are carried out. First, force strengths of two-body effective interactions among identical nucleons are adjusted to fit experimental data for singly closed nuclei. Next, quadrupole-quadrupole interactions between neutrons and protons for open shell nuclei are adjusted. The shell model results for the even-even isotopes $^{130-134}$Xe are examined in detail in Sec. III. In order to investigate collective behavior at low energies and the effect of the pair of two $0h_{11/2}$ neutrons at high spins, the energy spectra in the shell model are compared with those in the truncated SD collective space and those in the truncated $SD+(h_{11/2})^2$ space. The SD space is constructed by the S and D pairs, and the $SD+(h_{11/2})^2$ space by a neutron $(h_{11/2})^2$ pair in addition to the S and D pairs. The Hamiltonian in these truncated spaces is set identical to that used in the shell model. In Sec. IV, results reported in this paper are summarized and conclusions are drawn.

II. SHELL MODEL CALCULATIONS

All the relevant orbitals should be included in the original shell model space to describe a nucleus in the major shell between $50 \leqslant N(Z) \leqslant 82$. However, some kinds of truncation schemes are necessary since at present large-scale shell model calculations are infeasible for these medium-heavy nuclei.

From experimental excitation energies of the nuclei ^{131}Sn and ^{133}Sb [31,32], a relatively large level spacing is inferred between the levels $1d_{5/2}$ and $1d_{3/2}$, which is about 1.7 MeV for both the neutron and proton single-particle orbitals. In the Xe isotopes, with which we are concerned, the number of valence neutron holes is restricted to $N_\nu=0\sim6$ ($N_\pi=4$ for proton particles), so that the occupation probabilities of $1d_{3/2}$, $0h_{11/2}$, and $2s_{1/2}$ ($1d_{5/2}$ and $0g_{7/2}$) levels are expected to be larger for the neutron (proton) space. For instance, this fact can be readily confirmed by investigating the S-pair structure which composes the ground states. In Ref. [10] the structure of the S pair was determined in the full major shell to show that the occupation probabilities in the $1d_{3/2}$, $0h_{11/2}$, and $2s_{1/2}$ ($1d_{5/2}$ and $0g_{7/2}$) levels for neutron holes (proton particles) are dominant. Therefore, we assume the $N=Z=64$ subshell closure, and adopt the same single-particle orbitals given above in the present analyses.

The effective shell model Hamiltonian is written as

$$H=H_\nu+H_\pi+H_{\nu\pi}, \tag{1}$$

where H_ν, H_π, and $H_{\nu\pi}$ represent the neutron interaction, the proton interaction, and the neutron-proton interaction, respectively.

The interaction among like nucleons H_τ($\tau=\nu$ or π) consists of spherical single-particle energies, monopole-pairing interaction (P), quadrupole-pairing interaction ($P^{(2)}$), and quadrupole-quadrupole (QQ) interaction:

TABLE I. Adopted single-particle energies for neutron holes and proton particles, which are extracted from experiment [31,32] (in MeV).

j	$2s_{1/2}$	$0h_{11/2}$	$1d_{3/2}$	$1d_{5/2}$	$0g_{7/2}$
ε_ν	0.332	0.242	0.000		
ε_π				0.962	0.000

$$H_\tau=\sum_{jm}\varepsilon_{j\tau}c^\dagger_{jm\tau}c_{jm\tau}-G_{0\tau}P^{\dagger(0)}_\tau P^{(0)}_\tau - G_{2\tau}P^{\dagger(2)}_\tau\cdot\tilde{P}^{(2)}_\tau-\kappa_\tau{:}Q_\tau\cdot Q_\tau{:}, \tag{2}$$

where :: stands for normal ordering. Here $c^\dagger_{jm\tau}$ and $c_{jm\tau}$ are the nucleon creation and annihilation operators, respectively, and (j,m) represents a set of quantum numbers necessary to specify a single-particle state. The monopole-pairing operator $P^{\dagger(0)}_\tau$, the quadrupole-pairing operators $P^{\dagger(2)}_{M\tau}$, $\tilde{P}^{(2)}_{M\tau}$ and the quadrupole operator $Q_{M\tau}$ are defined as

$$P^{\dagger(0)}_\tau=\sum_j\frac{\sqrt{2j+1}}{2}A^{\dagger(0)}_{0\tau}(jj), \tag{3}$$

$$P^{\dagger(2)}_{M\tau}=\sum_{j_1j_2}Q_{j_1j_2}A^{\dagger(2)}_{M\tau}(j_1j_2), \tag{4}$$

$$\tilde{P}^{(2)}_{M\tau}=(-)^M P^{(2)}_{-M\tau}, \tag{5}$$

$$Q_{M\tau}=\sum_{j_1j_2}Q_{j_1j_2}[c^\dagger_{j_1\tau}\tilde{c}_{j_2\tau}]^{(2)}_M,$$

$$(\tilde{c}_{jm\tau}=(-1)^{j-m}c_{j-m\tau}), \tag{6}$$

$$Q_{j_1j_2}=-\frac{\langle j_1\|r^2Y^{(2)}\|j_2\rangle}{\sqrt{5}}, \tag{7}$$

where the creation operator of a pair of nucleons in orbitals j_1 and j_2 with total angular momentum J and magnetic quantum number M is constructed as

$$A^{\dagger(J)}_{M\tau}(j_1j_2)=\sum_{m_1m_2}(j_1m_1j_2m_2|JM)c^\dagger_{j_1m_1\tau}c^\dagger_{j_2m_2\tau} =[c^\dagger_{j_1\tau}c^\dagger_{j_2\tau}]^{(J)}_M. \tag{8}$$

The interaction between neutrons and protons $H_{\nu\pi}$ is taken as

$$H_{\nu\pi}=\kappa_{\nu\pi}Q_\nu\cdot Q_\pi. \tag{9}$$

Here the operator Q_τ is the quadrupole operator defined by Eq. (6). We employ the harmonic oscillator basis states with oscillator parameter $b=1$. The usage of these interactions was presented in Refs. [7–10].

The single-particle energies $\varepsilon_{j\tau}$ employed in the calculation are listed in Table I, which are extracted from experimental excitation energies in Refs. [31,32]. The single-

TABLE II. Force strengths used for Xe isotopes (in MeV).

	^{136}Xe	^{135}Xe	^{134}Xe	^{133}Xe	^{132}Xe	^{131}Xe	^{130}Xe
$G_{0\pi}$	0.200	0.200	0.200	0.200	0.200	0.200	0.200
$G_{2\pi}$	0.010	0.010	0.010	0.010	0.010	0.010	0.010
κ_{π}	0.080	0.080	0.080	0.080	0.080	0.080	0.080
$G_{0\nu}$			0.160	0.150	0.150	0.170	0.180
$G_{2\nu}$			0.012	0.008	0.004	0.006	0.006
κ_{ν}			0.160	0.160	0.160	0.120	0.160
$\kappa_{\nu\pi}$		0.240	0.200	0.180	0.160	0.100	0.120

particle energies are kept constant throughout all the Xe isotopes. The force strengths of two-body effective interactions are given in Table II. The method of determining force parameters is stated as follows.

First, two-body effective interactions among identical nucleons are fixed to reproduce experimental data for singly closed nuclei of ^{136}Xe and $^{126-131}$Sn. Secondly, force strengths of the $Q_{\nu}Q_{\pi}$ interactions between neutrons and protons $\kappa_{\nu\pi}$ are determined for open shell nuclei. Finally, the force strengths of the $Q_{\nu}Q_{\nu}$ interaction among neutrons κ_{ν} are slightly modified for a better fitting of high-spin states.

Some characteristics of the theoretical spectra are as follows. In the case of ^{130}Sn, the energy spectrum is not well reproduced. Especially the calculated excitation energies are rather higher than experimental ones.

The ground state of $3/2^+$ and the first excited state of $11/2^-$ are well reproduced in ^{131}Sn and ^{129}Sn. In case of ^{127}Sn, they are almost degenerate in experiment, but the separation is about 0.3 MeV in the calculation. The resulting order of the calculated energy levels is qualitatively explained as follows.

For the ground state of ^{131}Sn, one neutron hole occupies the $1d_{3/2}$ orbital. This state has the spin and parity $3/2^+$. For the ground state of ^{129}Sn, three neutron holes occupy the $1d_{3/2}$ orbital. Since two neutron holes compose a pair of spin and parity 0^+ and one neutron hole occupies the $1d_{3/2}$ orbital, this state has the spin and parity $3/2^+$. On the other hand, for the ground state of ^{127}Sn, five neutron holes cannot occupy the $1d_{3/2}$ orbital, because the $1d_{3/2}$ orbital is filled with four holes. Four neutron holes fully occupy the $1d_{3/2}$ orbital and one neutron hole occupies the $0h_{11/2}$ orbital. Thus, the ground state has the spin and parity $11/2^-$. The first excited state of ^{127}Sn has the spin and parity $3/2^+$, since a $1d_{3/2}$ neutron hole excited to the $0h_{11/2}$ orbital composes a 0^+ pair together with the partner in the $0h_{11/2}$ orbital, two holes in the $1d_{3/2}$ orbital compose a 0^+ pair, and one neutron hole remaining in the $1d_{3/2}$ orbital produces the total spin and parity $3/2^+$.

The force strengths of the pairing interaction are determined under the general assumptions on the nature of the residual interactions [33]

$$G \sim \frac{20 \text{ MeV}}{A}. \tag{10}$$

This gives $G \sim 0.15$ MeV for $A \sim 130$. Direct comparison of the present interactions with those in other approaches may be misleading because of the differences of the shell model spaces. However, it is recognized in Table II that our neutron pairing strengths $G_{0\nu}$ are close to this value, and proton pairing strengths $G_{0\pi}$ are slightly larger. The difference between the neutron and the proton pairing strengths given by Ref. [12], i.e., $G_{0\nu}=0.131$ MeV and $G_{0\pi}=0.180$ MeV, is similar to ours. Our pairing strengths are about 0.02 MeV larger than those in Ref. [12].

Concerning the QQ interactions, the force strengths chosen in the calculation are much larger compared to the previous studies (especially, κ_{ν} for the interactions among neutrons) [10–12]. With weaker QQ interactions, energy levels of high-spin yrast states cannot be reproduced. There are some calculations with stronger QQ interactions. For example, the NPSM calculation in the SD space uses the surface delta interaction among like nucleons and $Q_{\nu}Q_{\pi}$ interaction between neutrons and protons [14]. Their force strengths of the $Q_{\nu}Q_{\pi}$ interaction are similar to ours in magnitude.

The theoretical and experimental spectra for positive parity levels are compared in Fig. 1. In ^{136}Xe, which is a singly closed shell nucleus, the yrast 6^+ state comes close to the 4^+ state in the calculation. This is characteristic of our effective interactions of the $P+QQ$ type. If we intend to describe the level spacing between these two states more precisely, we need higher multipole interactions in the Hamiltonian, such as a hexadecapole-pairing interaction, a hexadecapole-hexadecapole interaction, and so on.

In ^{134}Xe, the level spacing between the yrast 4^+ and 6^+ states is small, and the yrast 8^+ and 10^+ states are almost degenerate in experiment. Our theoretical energy levels match the irregularities of the experimental data, and achieve sufficiently good agreement. The 2^+ state on the quasi-γ band is a bit lower and the 3_1^+ state is somewhat higher in our calculation than experiment. The calculated 0_2^+ state appears lower in energy, due to the facts that the $P+QQ$ interaction is oversimplified and the yrast band is mainly focused on determining force parameters.

In ^{132}Xe, energy levels of the even-spin yrast band and the quasi-γ band are reasonably well reproduced, and our calculation predicts that the yrast 10^+ state should come below 8^+ states. This is consistent with the following experimental evidence. The $10^+ \rightarrow 8^+$ isomeric transitions for ^{130}Te, ^{132}Te, ^{130}Xe, and ^{134}Xe were reported in Refs. [35,36]. Their half-lives of the 10^+ isomers are $T_{1/2}=1.90(8)$ μs, 3.70(9) μs, 5.9(8) ns, and 5(1) μs for ^{130}Te, ^{132}Te, ^{130}Xe, and ^{134}Xe, respectively. On the other hand, in case of ^{132}Xe, the 10^+ isomer decays into the 7^- level by the unique transition of $E3$ multipolarity and has the long half-life of $T_{1/2}=8.4$ ms [37]. This fact indicates that our calculation yields consistent results along the yrast sequence, predicting the unknown 8_1^+ state to appear above the 10_1^+ state about 0.05 MeV.

In ^{130}Xe, the even-spin yrast sequence is well reproduced except for the 8^+ state, which is lower than experiment. The calculated quasi-γ band appears somewhat higher in energy than experiment, but the result is satisfactory. Especially, the energy staggering of even-odd spin states on the quasi-γ band is well reproduced.

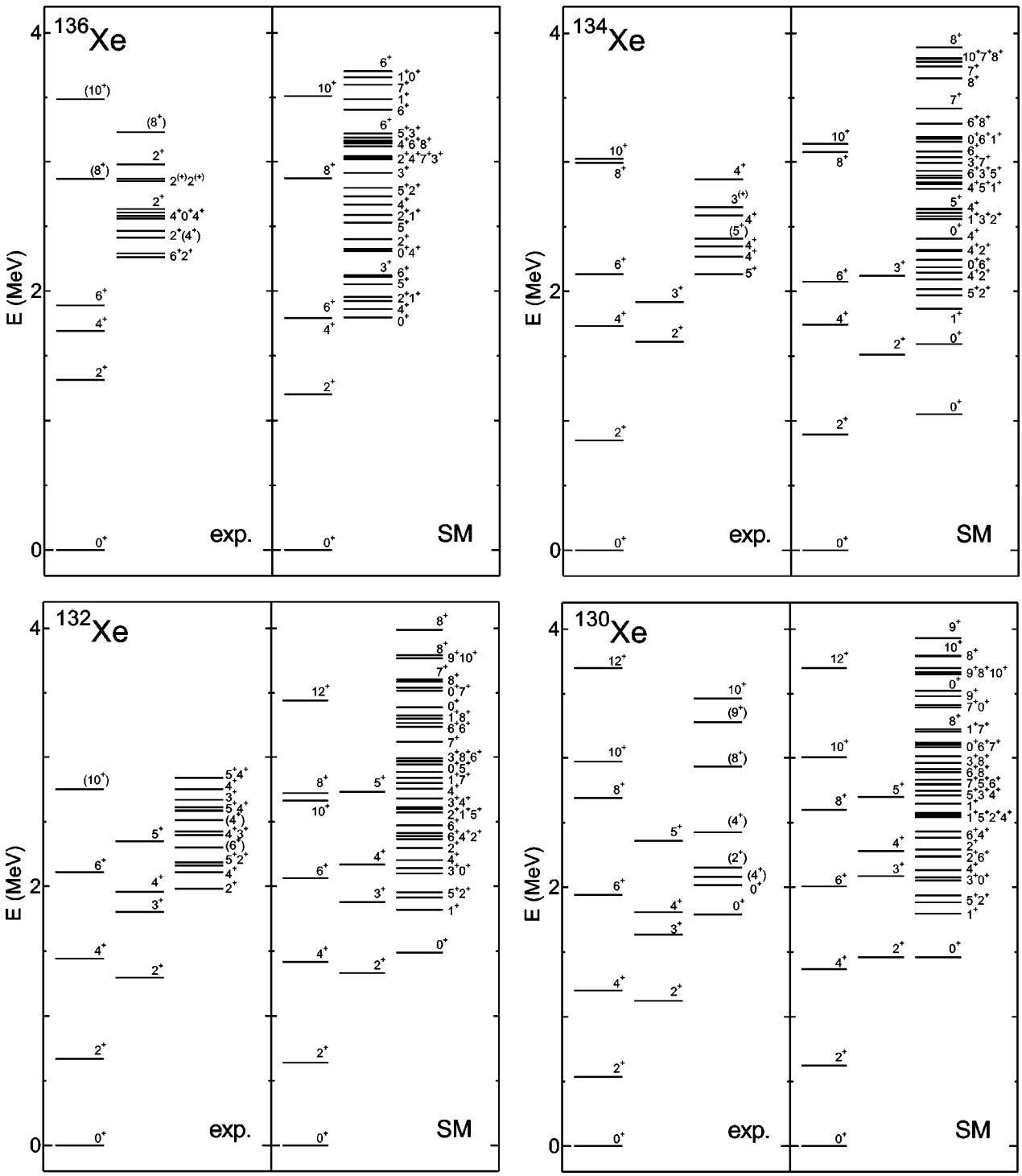

FIG. 1. Comparison of energy spectra in experiment (exp.) with the shell model (SM) results for the even-even isotopes $^{130-136}$Xe. The experimental data are taken from Refs. [34–37].

In even-even isotopes $^{130-134}$Xe, experimental γ-ray energies versus angular momentum I are compared with the shell model results along the yrast sequence in Fig. 2. In this figure for ^{132}Xe, we use the experimental excitation energies of the yrast 10^+ state instead of the yrast 8^+ state since the 8^+ states are not yet known experimentally. On the other hand, for ^{130}Xe and ^{134}Xe, the excitation energies of the 8_1^+ states are available since these states were observed at around 2.9 MeV [35,36]. The calculated levels agree with experimental ones, especially the sudden decrease of level spacing occurring around the states of spin 10^+ is well reproduced for all of these isotopes.

In Fig. 3 the calculated yrast levels are compared with the experimental data for odd isotopes $^{131-135}$Xe. It is recognized that yrast levels are well reproduced except for low-lying negative parity states in ^{131}Xe. The negative parity states

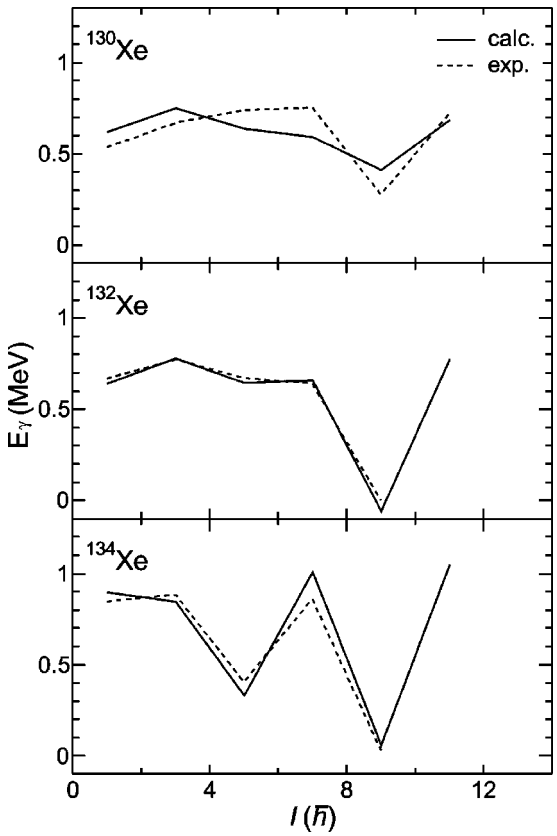

FIG. 2. Comparison of γ-ray energies $E_\gamma[E_\gamma = E(I+1) - E(I-1)]$ versus angular momentum I in experiment (exp.) with the shell model (SM) results for even-even isotopes $^{130-134}$Xe. The experimental data are taken from Refs. [34–37].

appear lower in energy than those of positive parity states due to the energy difference between the ground $11/2^-$ and the first excited $3/2^+$ states in ^{127}Sn. A simple modification of force strengths of the present scheme turns out to be insufficient for changing the order. For this inversion, it is necessary either to shift the $h_{11/2}$ single-particle energy relative to the others or to modify the force strength of $Q_\nu Q_\nu$ related to the $h_{11/2}$ orbital.

III. THE ANALYSIS OF THE SHELL MODEL RESULTS

Throughout the great successes of the IBM, it has been understood from a microscopic consideration that nucleon pairs with low angular momenta play essential roles in nuclear collective motion. Therefore it is natural to expect that the *SD*-pair model works well in describing low-lying states. In this model, nuclear collective excitations are described by the *S*- and *D*-nucleon collective pairs.

Using the two-nucleon creation operators $A_M^{\dagger(J)}$ as defined in Eq. (8), we give the *S* and *D* pairs in terms of the linear combinations of $A_M^{\dagger(J)}$,

$$S^\dagger = \sum_j \alpha_j A_0^{\dagger(0)}(jj), \tag{11}$$

$$D_M^\dagger = \sum_{j_1 j_2} \beta_{j_1 j_2} A_M^{\dagger(2)}(j_1 j_2). \tag{12}$$

The structure coefficients α and β are determined so as to maximize the collectivity of the *S* and *D* pairs. More explicitly, the structure of the collective *S* pair is determined by the variation

$$\delta\langle S^N|H|S^N\rangle = 0, \tag{13}$$

which is considered as a number conserved BCS equation. In the second step, with the use of the *S* pair obtained above, the structure of the collective *D* pair is determined by

$$\delta\langle S^{N-1}D|H|S^{N-1}D\rangle = 0. \tag{14}$$

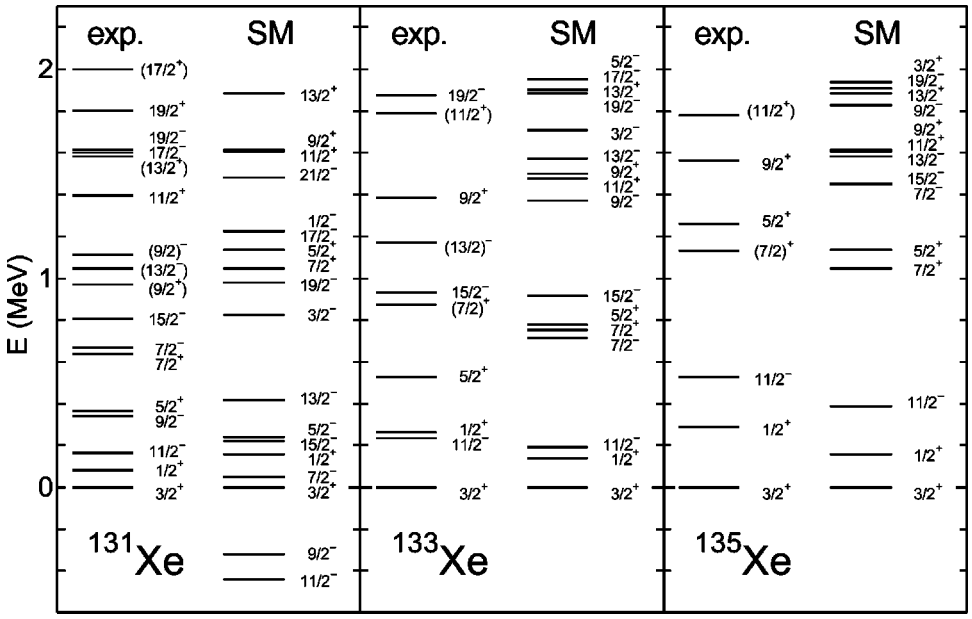

FIG. 3. Comparison of energy spectra in experiment (exp.) with the shell model (SM) results for odd isotopes $^{131-135}$Xe. The experimental data are taken from Ref. [34].

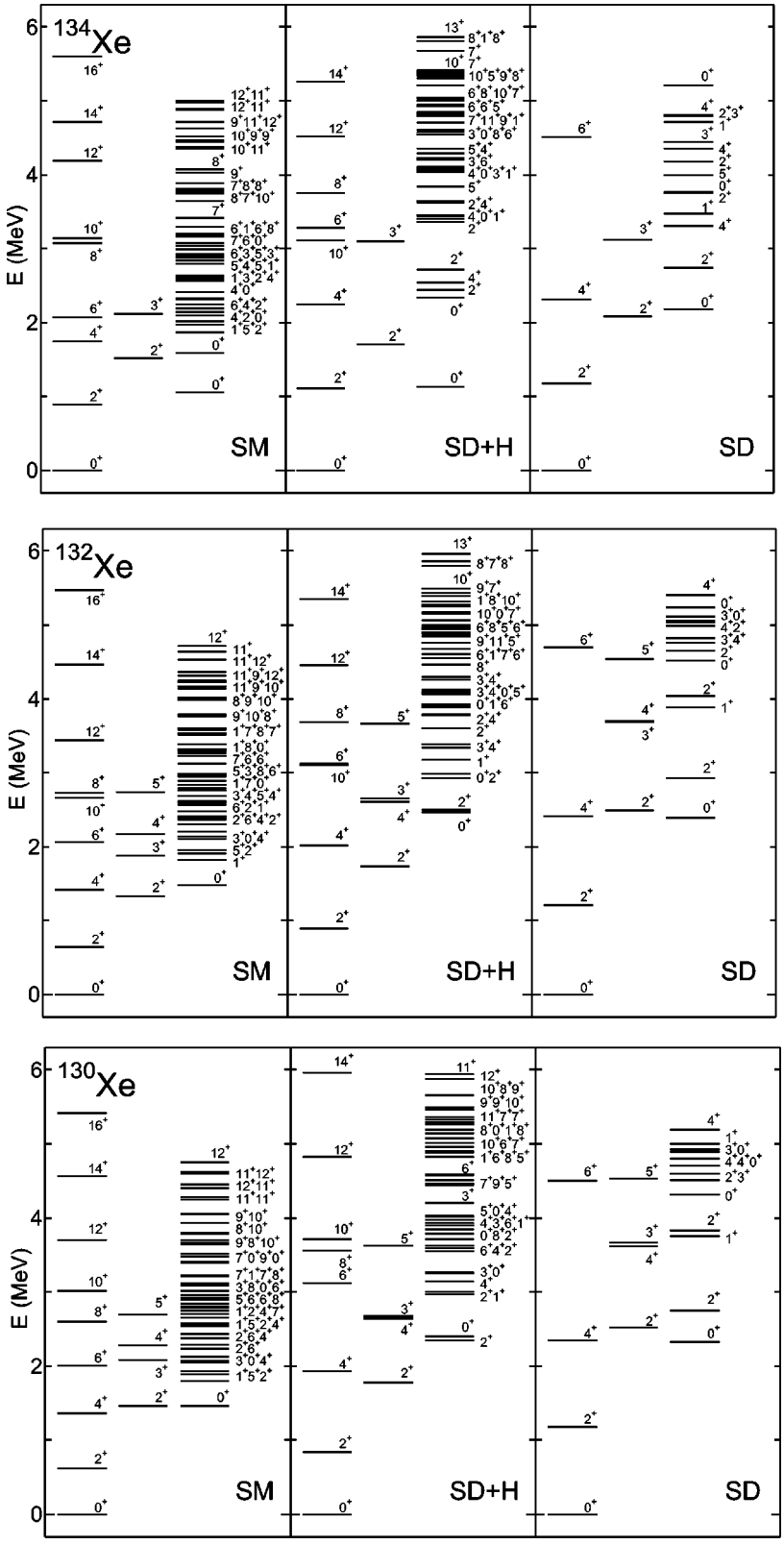

FIG. 4. Comparison of energy spectra between the shell model (SM), *SD*- and *SD*+*H*-pair models for the even-even isotopes $^{130-134}$Xe.

After determining the structure of the S and D pairs, the collective states of even-even nuclei are constructed on the core $|-\rangle$ as

$$(S^\dagger)^{n_s}(D^\dagger)^{n_d}|-\rangle=|S^{n_s}D^{n_d}\quad \eta I\rangle, \tag{15}$$

where η is an additional quantum number required to completely specify the states and I a total angular momentum of the nuclear state. Here, the number of valence nucleon pairs n_s+n_d is fixed constant for a specific nucleus. The SD-pair states are generally nonorthogonal and the Schmidt orthogonalization procedure is necessary. The detailed prescriptions for the SD-pair model have been given in Refs. [8–10].

In the present paper we propose the $SD+(h_{11/2})^2$-pair model, which includes a pair of neutrons in the $0h_{11/2}$ orbital in addition to the ordinary S and D pairs. The reason why the $(h_{11/2})^2$ pair should be incorporated in the SD-pair model is stated as follows. From various experimental investigations [38,39], it is inferred that the spin alignment of two neutrons in the $0h_{11/2}$ orbital, the intruder high-j orbital in $A\sim130$ region, contributes to the determination of the yrast 10^+ configuration, and gives rise to backbending. Hence, the $SD+(h_{11/2})^2$-pair model is expected to work thoroughly in both the high-spin states and the low-spin states within a common framework.

The $(h_{11/2})^2$-pair creation operators are defined as

$$H_M^{\dagger(J)}=[c_{11/2}^\dagger\ \ c_{11/2}^\dagger]_M^{(J)}, \tag{16}$$

with $J=0$, 2, 4, 6, 8, and 10. Note that the $(h_{11/2})^2$ pair has a unique structure in contrast to the S and D pairs, and has some overlap with S or D pairs for $J=0$ or $J=2$, respectively. The $(h_{11/2})^2$ pair is shortly denoted as the H pair, hereafter. In the $(SD+H)$-pair model, the nuclear states of even-even nuclei are described by the states

$$(S^\dagger)^{n_s}(D^\dagger)^{n_d}(H^\dagger)^{n_h}|-\rangle=|S^{n_s}D^{n_d}H^{n_h}\quad \eta I\rangle, \tag{17}$$

where η and I denote the same as in the SD-pair model, and $n_s+n_d+n_h$ gives the number of nucleon pairs. In the present calculation, the number of the H pairs is limited to at most one (i.e., $n_h=0$ or 1). Thus, the states of even-even nuclei are constructed as linear combinations of $|S_\nu^{n_{s\nu}}D_\nu^{n_{d\nu}}H_\nu\ S_\pi^{n_{s\pi}}D_\pi^{n_{d\pi}}\ \eta I\rangle$ and $|S_\nu^{n_{s\nu}}D_\nu^{n_{d\nu}}\ S_\pi^{n_{s\pi}}D_\pi^{n_{d\pi}}\ \eta I\rangle$.

We calculate energy spectra in the SD- and $(SD+H)$-pair models using the Hamiltonian identical to the one employed in the shell model calculations. They are compared with the shell model results for the even-even isotopes $^{130-134}$Xe in Fig. 4.

For each nucleus, the yrast 6^+ and 8^+ states in the $(SD+H)$-pair model are shifted further upward than those in the shell model, while the yrast 10^+ states appear almost at the same position in both models. This is due to the fact that the 10_1^+ state can be reproduced mainly by an H pair, but the 6_1^+ and 8_1^+ states have much more complicated structure and require the dissociation of the S and D pairs to form higher angular momentum pairs, such as G pairs. The energy levels of the quasi-γ bands are nicely reproduced. Although the $(SD+H)$-pair model gives a sharper backbending compared to the shell model, its results are still much better than those in the SD-pair model, especially at high spins. The expectation values of the numbers of D and H pairs in the yrast sequence are listed in Table III. There we also see that the S and D pairs are dominant in low-lying states, and the effect of the H pair is large above 8^+ states. Comparing the SD-pair model with the shell model, a qualitative agreement is generally achieved in the low-lying states. Especially, the even-odd staggering in the quasi-γ band is well reproduced. This implies that the low-lying states consist mainly of S and D pairs, and the SD truncation scheme [10–14] provides us with an efficient and practical method in the $A\sim130$ region.

IV. SUMMARY AND CONCLUSION

It is one of our purposes to propose a shell model description of high-spin phenomena which are caused by the interplays between quadrupole collective motion and the excitation of single-particle degrees of freedom in medium-heavy nuclei. In this paper, we have successfully demonstrated the capability of the shell model by showing the theoretical results for Xe isotopes in the $A\sim130$ region.

The calculated spectra are nicely fitted to experimental data for high-spin states as well as low-lying states, and the backbending is well reproduced for the even-even isotopes $^{130-134}$Xe. Particularly, the complicated yrast band levels are well reproduced for ^{132}Xe and ^{134}Xe. In ^{132}Xe, the experimental half-life $T_{1/2}=8.4$ ms of the yrast 10^+ state is much longer compared to other nuclei. This suggests that the experimentally unconfirmed 8_1^+ state exists above the 10_1^+ state. Our calculation predicts that the yrast 8^+ state exists at an excitation energy about 0.05 MeV higher than the 10_1^+ state. This is the first successful description of such an irregularity in terms of the shell model framework. Concerning ^{130}Xe and ^{132}Xe, our calculations reproduce the energy staggering of even-odd spin states on the quasi-γ band, which indicates the instability of a deformed potential in the γ direction. The reproduction of the yrast band is satisfactory also for odd mass nuclei except for ^{131}Xe, in which negative parity states come lower in energy. In order to fit the theoretical spectra to experiment, we have chosen much stronger force strengths of the $Q_\nu Q_\nu$ interaction among neutrons. Although inclusion of higher multipole interactions may be de-

TABLE III. The expectation numbers of the D and H pairs calculated in the $SD+H$ pair model. The number of D pairs are the sum of the neutron D_ν pairs and the proton D_π pairs $(n_{d\nu}+n_{d\pi})$.

	^{130}Xe		^{132}Xe		^{134}Xe	
I^π	H	D	H	D	H	D
12^+	1.00	1.81	1.00	1.58	1.00	1.23
10^+	1.00	1.10	1.00	0.76	1.00	0.34
8^+	0.99	1.18	1.00	0.94	1.00	0.55
6^+	0.69	2.12	0.92	1.17	0.94	0.64
4^+	0.30	2.24	0.48	1.64	0.36	1.85
2^+	0.16	1.72	0.22	1.44	0.12	1.09
0^+	0.06	1.22	0.09	0.98	0.07	0.35

sirable to obtain a better fit, we have avoided such a complication as much as possible in the present analyses since we concentrate on clarifying the role of the intruder orbital within the shell model framework.

In order to interpret the shell model results, we have compared those with the SD- and $(SD+H)$-pair model results. The SD-pair truncation reduces the shell model dimension drastically. In the $(SD+H)$-pair model, a pair of neutrons in the $0h_{11/2}$ orbital is taken into account in addition to the S and D pairs. We have kept using the same Hamiltonian as adopted for the shell model calculation, since our aim in these calculations is to interpret the shell model results rather than to describe the experimental spectra in terms of the pair-truncated models. It has been shown that the SD-pair calculations qualitatively reproduce the shell model results at low energy, while the $(SD+H)$-pair model improves the SD-pair model substantially and is in quantitative agreement with the shell model results from low spins to high spins. It is found that the SD collective nucleon pairs play essential roles in describing the low-lying states, and the pair of $h_{11/2}$ neutrons is indispensable for the high-spin states around the backbending region.

ACKNOWLEDGMENTS

The authors would like to thank Drs. K. Enami, Y. M. Zhao, and A. Gelberg for valuable discussions. This work was supported in part by Grant-in-Aid for Scientific Research (C) (Grant No. 13640262).

[1] F. Iachello and A. Arima, *The Interacting Boson Model* (Cambridge University, Cambridge, 1987).
[2] R.F. Casten and P. von Brentano, Phys. Lett. **152B**, 22 (1985).
[3] G. Puddu, O. Scholten, and T. Otsuka, Nucl. Phys. **A348**, 109 (1980).
[4] X.W. Pan, J.L. Ping, D.H. Feng, J.Q. Chen, C.L. Wu, and M.W. Guidry, Phys. Rev. C **53**, 715 (1996).
[5] J.Q. Chen, Nucl. Phys. **A626**, 686 (1997).
[6] Y.M. Zhao, N. Yoshinaga, S. Yamaji, J.Q. Chen, and A. Arima, Phys. Rev. C **62**, 014304 (2000).
[7] N. Yoshinaga and D.M. Brink, Nucl. Phys. **A515**, 1 (1990).
[8] N. Yoshinaga, Nucl. Phys. **A570**, 421 (1994).
[9] N. Yoshinaga, T. Mizusaki, A. Arima, and Y.D. Devi, Prog. Theor. Phys. Suppl. **125**, 65 (1996).
[10] N. Yoshinaga, Y.D. Devi, and A. Arima, Phys. Rev. C **62**, 024309 (2000).
[11] T. Mizusaki and T. Otsuka, Prog. Theor. Phys. Suppl. **125**, 97 (1996).
[12] Y.M. Zhao, S. Yamaji, N. Yoshinaga, and A. Arima, Phys. Rev. C **62**, 014315 (2000).
[13] Y.A. Luo and J.Q. Chen, Phys. Rev. C **58**, 589 (1998).
[14] Y.A. Luo, J.Q. Chen, and J.P. Draayer, Nucl. Phys. **A669**, 101 (2000).
[15] Y.M. Zhao, N. Yoshinaga, S. Yamaji, and A. Arima, Phys. Rev. C **62**, 014316 (2000).
[16] K. Tanabe and K. Sugawara-Tanabe, Phys. Lett. **135B**, 353 (1984).
[17] K. Tanabe and K. Sugawara-Tanabe, Phys. Lett. B **259**, 12 (1991).
[18] K. Enami, K. Tanabe, and N. Yoshinaga, Phys. Rev. C **59**, 135 (1999).
[19] K. Enami, K. Tanabe, and N. Yoshinaga, Phys. Rev. C **61**, 027301 (2000).
[20] J.L. Egido and L.M. Robledo, Phys. Rev. Lett. **70**, 2876 (1993).
[21] E. Garrote, J.L. Egido, and L.M. Robledo, Phys. Rev. Lett. **80**, 4398 (1998).
[22] J. Fleckner, U. Mosel, P. Ring, and H.J. Mang, Nucl. Phys. **A331**, 288 (1979).
[23] P. Bonche, P.H. Heenen, and H.C. Flocard, Nucl. Phys. **A467**, 115 (1987).
[24] E. Caurier, J.L. Egido, G. Martinez-Pinedo, A. Poves, J. Retamosa, L.M. Robledo, and A.P. Zuker, Phys. Rev. Lett. **75**, 2466 (1995).
[25] G. Martinez-Pinedo, A. Poves, L.M. Robledo, E. Caurier, F. Nowacki, J. Retamosa, and A. Zuker, Phys. Rev. C **54**, R2150 (1996).
[26] K. Hara, Y. Sun, and T. Mizusaki, Phys. Rev. Lett. **83**, 1922 (1999).
[27] A. Gelberg and A. Zemel, Phys. Rev. C **22**, 937 (1980).
[28] N. Yoshida, A. Arima, and T. Otsuka, Phys. Lett. **164B**, 231 (1982).
[29] H. Kusakari and M. Sugawara, Z. Phys. A **317**, 287 (1984).
[30] A. Gelberg, N. Yoshida, T. Otsuka, A. Arima, A. Gade, A. Dewald, and P. von Brentano, in *Quasiparticle and Phonon Excitations in Nuclei (Soloviev 99)*, edited by N. Dang and A. Arima (World Scientific, Singapore, 1999), p. 100.
[31] B. Fogelberg and J. Blomqvist, Nucl. Phys. **A429**, 205 (1984).
[32] M. Sanchez-Vega, B. Fogelberg, H. Mach, R.B.E. Taylor, A. Lindroth, J. Blomqvist, A. Covello, and A. Gargano, Phys. Rev. C **60**, 024303 (1999).
[33] D. R. Bes and R. A. Sorensen, in *Advance in Nuclear Physics*, edited by M. Baranger and E. Vogt (Plenum, New York, 1969), Vol. 2, p. 129.
[34] R. B. Firestone, V. S. Shirley, C. M. Baglin, S. Y. F. Chu, and J. Zipkin, *Table of Isotopes* (Wiley, New York, 1996).
[35] H. Kusakari, K. Kitao, K. Sato, M. Sugawara, and H. Katsuragawa, Nucl. Phys. **A401**, 445 (1983).
[36] J. Genevey, J.A. Pinston, C. Foin, M. Rejmund, R.F. Casten, H. Faust, and S. Oberstedt, Phys. Rev. C **63**, 054315 (2001).
[37] A. Kerek, A. Luukko, M. Grecescu, and J. Sztarkier, Nucl. Phys. **A172**, 603 (1971).
[38] H. Kusakari, M. Sugawara, M. Fujioka, N. Kawamura, S. Hayashibe, K. Iura, F. Sakai, and T. Ishimatsu, Phys. Rev. C **30**, 820 (1984).
[39] P. Das, R.G. Pillay, V.V. Krishnamurthy, S.N. Mishra, and S.H. Devare, Phys. Rev. C **53**, 1009 (1996).